Structural analysis and parametric study ballasted track in sandy regions

Xiao, Hong; Zhang, Zhihai; Chi, Yihao; Wang, Xiaoyu; Wang, Haoyu; Jiang, Ziqing

DOI
10.1016/j.conbuildmat.2022.127439

Publication date
2022

Document Version
Final published version

Published in
Construction and Building Materials

Citation (APA)
Xiao, H., Zhang, Z., Chi, Y., Wang, X., Wang, H., & Jiang, Z. (2022). Structural analysis and parametric study ballasted track in sandy regions. *Construction and Building Materials*, *333*, Article 127439. https://doi.org/10.1016/j.conbuildmat.2022.127439

Construction and Building Materials 333 (2022) 127439

Contents lists available at ScienceDirect

Construction and Building Materials

journal homepage: www.elsevier.com/locate/conbuildmat

Structural analysis and parametric study ballasted track in sandy regions

Hong Xiao [a,b,*], Zhihai Zhang [a,b,*], Yihao Chi [a,b], Xiaoyu Wang [a,b], Haoyu Wang [c], Ziqing Jiang [d]

[a] School of Civil Engineering, Beijing Jiaotong University, Beijing 100044, China
[b] Beijing Key Laboratory of Track Engineering, Beijing Jiaotong University, Beijing 100044, China
[c] Engineering Structures Department, Delft University of Technology, the Netherlands
[d] China Academy of Railway Sciences Co., Ltd., Beijing 100081, China

ARTICLE INFO

Keywords:
Desert railway
Ballasted track
Discrete element method
Contact force
Vibration acceleration

ABSTRACT

The sand intrusion in railway tracks in sandy regions can significantly change the mechanical behaviour of tracks and thus threaten the safety of train operation. This paper presents substantial field tests on both sandy and clean railway tracks to study the effect of sand intrusion on the longitudinal resistance of ballast bed and the vibration behaviour of track structures. After that, a 3D multi-scale the discrete element model is developed to study the micro-contact between ballast particles and the vibration behaviour of sandy tracks during train passing in detail. Also, the effect of train speeds and axle loads on the mechanical behaviour of sandy tracks is discussed. The results show that the sand intrusion increases the vibration acceleration amplitude of rail and sleeper by 11.3% and 50.3%, while ballast bed decreases by 44.9%. Besides, the sand intrusion significantly changes the energy distribution in the track, wherein the frequencies of the highest energy of rail and sleeper are increased while that of the ballast bed is decreased. The parametric study shows the high train speed can cause the increase in overall acceleration of the ballast bed and high axle load can cause an increase in the micro-contact forces between ballast particles, diffusion angle of the contact force chain, displacements of ballast particles, acceleration of ballast particles, and sleeper displacements.

1. Introduction

Due to the material property of ballast particles, there are unavoidably many voids in the ballast bed of railways [1–3]. The voids can be filled by fouling materials during train operation, as shown in Fig. 1, including: (1) sand particles, dust particles, leaves, coal powders deposited on the top of tracks brought by trains or environment; (2) crushed or abrased ballast particles under cyclic train loads; (3) slurry gushed from soft-soil subgrade [4,5]. The fouling materials weaken the mechanical behaviour of the ballast bed and consequently affect track stability and operation safety [6]. As a result, it often takes considerably manpower and cost to maintain the fouled ballast bed, wherein the maintenance activities are commonly ballast cleaning, ballast replacement, or tamping activities. Therefore, the research on the performance of tracks with fouled ballast beds is important.

In the past few decades, many studies on the fouled ballast caused by crushed or abrased ballast particles and coal powder have been conducted [4–8]. However, the studies on the fouled ballast caused by sand particles are rare [9,10]. The difference between sand particles and other pollutants, e.g., coal powder and dust, is large in terms of stiffness, particle size and shape. Also, research shows the intrusion of sand particles can cause fastener corrosion, depressed joints, and large twist values, which reduces the longitudinal stability of tracks, deteriorates the track geometry, and affect track performance [10–12]. Therefore, it is of great importance to study the changes in the mechanical behaviour of the railway track caused by the sand intrusion.

The existing research on sandy tracks can be divided into experimental and numerical analyses.

1.1. Experimental analysis

Xiao et al. [2] conducted the laboratory test and found that the angle of repose of sand particles is 33.02°. Sadeghi et al. [11,12] analyzed the influence of sand content and water content on ballast behaviour by conducting a large-scale direct shear test and a plate load test and found that shear strength and vertical stiffness of sandy ballast can be significantly improved by the geogrid reinforcement. Akbar et al. [13] explored the influence of ballast gradation on the shear strength of sandy ballast beds and found that sand intrusion reduces the shear strength of ballast. Similar findings have been provided by Tolou Kian et al. [14–16]

* Corresponding authors at: School of Civil Engineering, Beijing Jiaotong University, Beijing 100044, China.
E-mail addresses: xiaoh@bjtu.edu.cn (H. Xiao), chenxizhang0912@163.com (Z. Zhang).

https://doi.org/10.1016/j.conbuildmat.2022.127439
Received 9 February 2022; Received in revised form 24 March 2022; Accepted 6 April 2022
Available online 11 April 2022

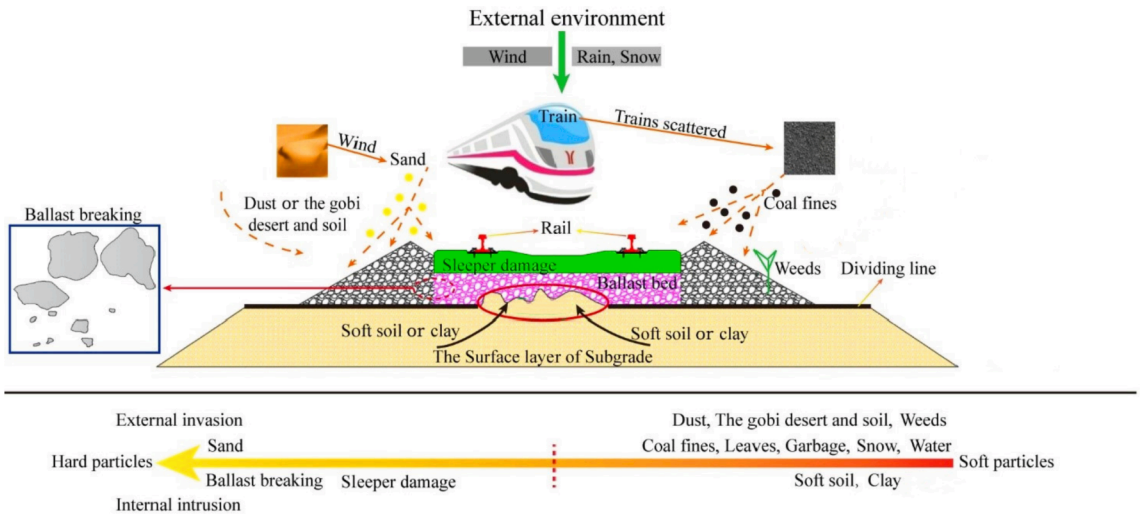

Fig. 1. Formation of ballast fouling and the classification.

after conducting laboratory experiments. In addition, it has been found that sand intrusion also reduces the deformation modulus of ballast beds. Zakeri et al. [17,18] carried out field tests and found the sand intrusion can change the load sharing ratio of a single sleeper. In research carried out by Koohmishi et al. [19], a series of large-scale permeability tests on the various gradation of clean ballast beds and the ballast beds with various sand content were conducted. The results showed that the clean ballast bed with evenly distributed gradation has the highest permeability. Esmaeili et al. [20–22] conducted 6-month monitoring on the track stiffness and ballast fouling rate of sandy tracks in the desert area and laboratory tests of the effect of water content on the mechanical behaviour of sandy ballast bed. The results show that the increase in sand content of the ballast bed reduces the damping ratio of the ballast bed. When the water content is between 0% and 15%, the loading period required for the cumulative settlement of the sandy ballast bed to stabilize is shortened. Tyfour et al. [23] found that sand can hinder the movement of ballast particles by filling the gaps between them, thereby increasing track stiffness and damping and furthermore aggravating the development of rail corrugation.

As seen from the above, it can be found that the experimental studies on sandy railways mainly focus on static laboratory tests, while field tests have been less conducted. In particular, there is a lack of research on the longitudinal resistance of sandy ballast bed and the vibration behaviour of sandy track structures.

1.2. Numerical analysis

Tolou Kian et al. [16] explored the influence of sand intrusion on the load mode of prestressed concrete sleepers using the finite element method. Esmaeili et al. [20] conducted the effect of sand intrusion on environmental vibration along railways using the finite element method. The results showed that the environmental vibration along with

Fig. 2. Site conditions: (a) sandy section, (b) clean section, (c) Front view of train operation direction, (d) Back view of train operation direction.

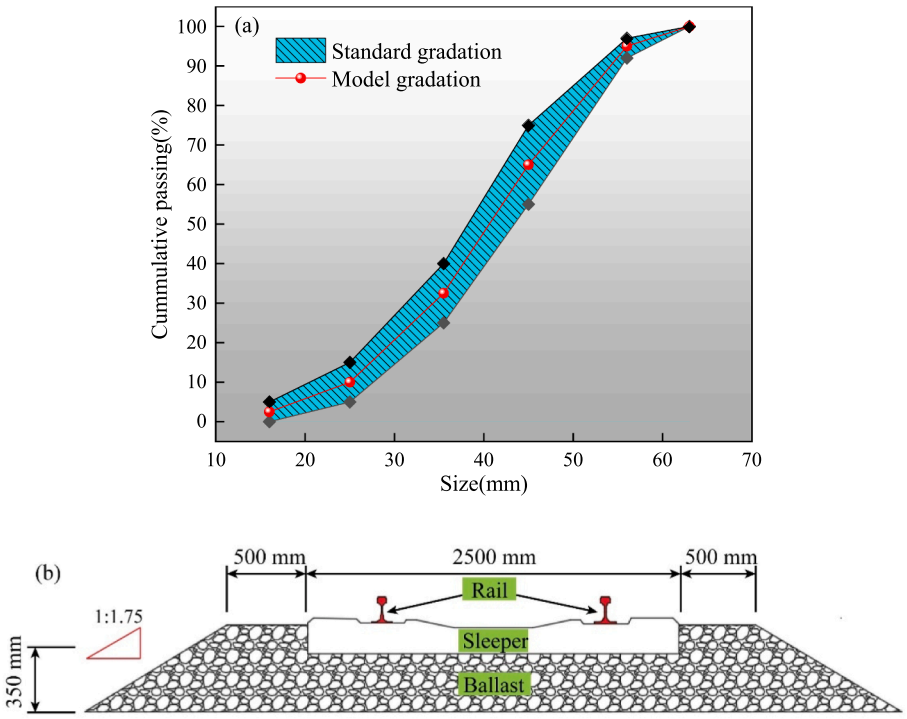

Fig. 3. Track structure at test site: (a) Ballast gradation, (b) track dimension.

railways increases as the sand content increases. Zakeri et al. [24] analyzed the structural response of sandy track under trainloads using a 2D finite element model and found that the vertical acceleration of track increases as the sand invasion. Xiao et al. and Zhang et al. [2,4] conducted the effect of sand intrusion on the stress in ballast and displacement of ballast particles using 2D discrete element methods.

It can be seen from the above, the existing numerical studies on sandy tracks have mostly used the finite element method while partly the discrete element method. Even the ones that use discrete element methods have only modelled the track in 2D models, which is difficult to analyze the micro-contact between the 3D ballast particles and sand particles. Besides, the influence of train speed and axle load on sandy tracks is still unknown.

Aiming at the deficiencies of existing experimental and numerical research, this paper presents substantial field tests on both sandy and clean railway tracks to study the effect of sand intrusion on the longitudinal resistance of track beds and the vibration behaviour of track structures. Besides, a 3D multi-scale discrete element model is developed to study the micro-contact between ballast particles and the vibration behaviour of sandy track under various train speeds and axle loads. The findings can provide a theoretical basis and technical guidance for the operation and maintenance of sandy railways.

2. Experimental analysis

2.1. Test object

To study the effect of sand intrusion on the longitudinal resistance of ballast bed and the vibration behaviour of track structures, field tests have been conducted at a sandy section and a clean section in a railway in the desert. The railway is named Ganqimaodu-Wanshuiquan Railway and is located in the north part of China. The test sections are shown in Fig. 2.

The test track is designed according to China's Class I existing railway and the ballast gradation meets the requirement of China's Class I existing railway [25], as shown in Fig. 3 (a). The width of the top and the thickness of the ballast bed is 3500 mm and 350 mm, respectively. The slope of the ballast bed is 1:1.75 and the width of the ballast shoulder is 500 mm, as shown in Fig. 3 (b). The sleeper is the Type II concrete sleeper, the dimension of which is 2500 mm × 280 mm × 205 mm (length × width × height). The sleeper spacing is 600 mm. The type of rail in the track is CHN60N (60.64 kg/m) and the fastener is the Type II clip fastening system.

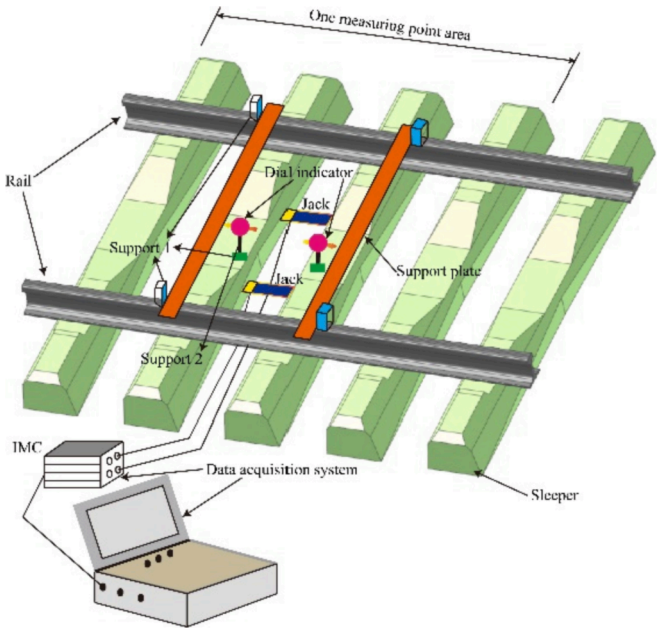

Fig. 4. Test principle of ballast bed longitudinal resistance.

The main type of operated train is C70E, with a wheel distance of 1830 mm and a bogie distance of 19100 mm. Its axle load is around 23 t and the operational speed is 45 km/h.

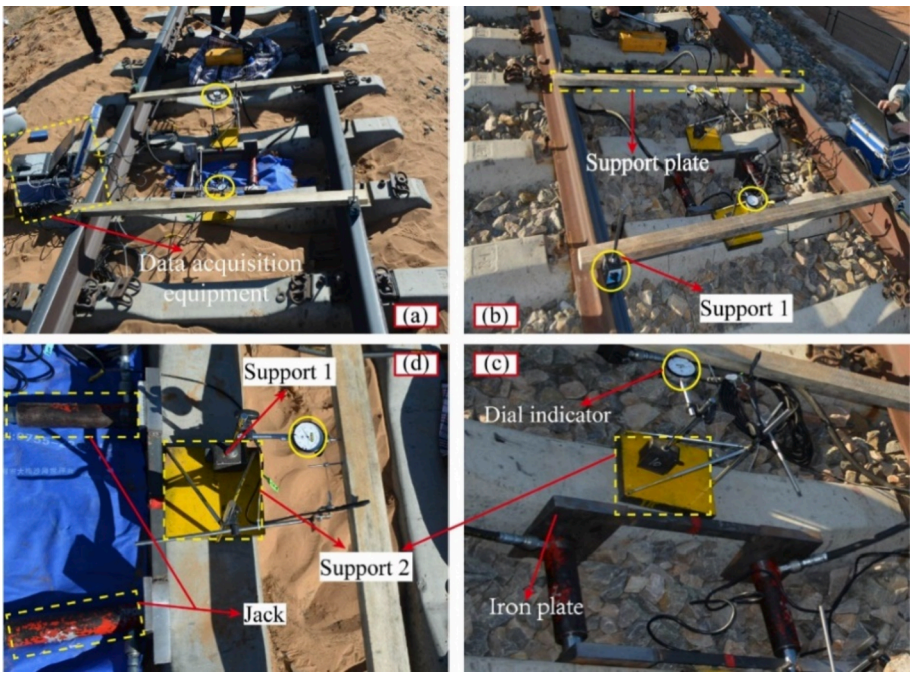

Fig. 5. Setup for longitudinal resistance test: (a) Sandy section, (b) Clean section, (c) Clean section equipment installation detail, (d) Sandy section equipment installation detail.

2.2. Test methods and procedures

2.2.1. Longitudinal resistance test of ballast bed

In the longitudinal resistance test, the sandy section and the clean section are tested respectively, with 5 different measuring points for each. At each measuring point, the interval measurement method is adopted, namely, the two middle sleepers out of four are tested. The longitudinal resistance test system is composed of hydraulic jacks, dial indicators, high-precision displacement sensors, a data acquisition system and support plates, which can measure the longitudinal displacement and force of the sleeper as shown in Fig. 4. Before testing, it is necessary to remove the fasteners and rail pads connecting to the tested sleeper. After that, two high-precision displacement sensors are installed at the top of the sleeper using a counterforce device and fixed by magnetic bases and iron plates. The high-precision displacement sensors measure the relative displacement between rail and sleeper. To prevent the sleeper from rotating during the test, two hydraulic jacks are placed at the middle height of the sleeper and symmetrically along the track center line. Then the hydraulic jacks slowly thrust the sleeper in the longitudinal direction, while the data acquisition system records the longitudinal forces and displacements measured by dial indicators [26,27]. Furthermore, it should be noted that the two hydraulic jacks are controlled by a pressure valve to realize synchronous loading. The sleepers on both sides of the jack move smoothly with the rail as the

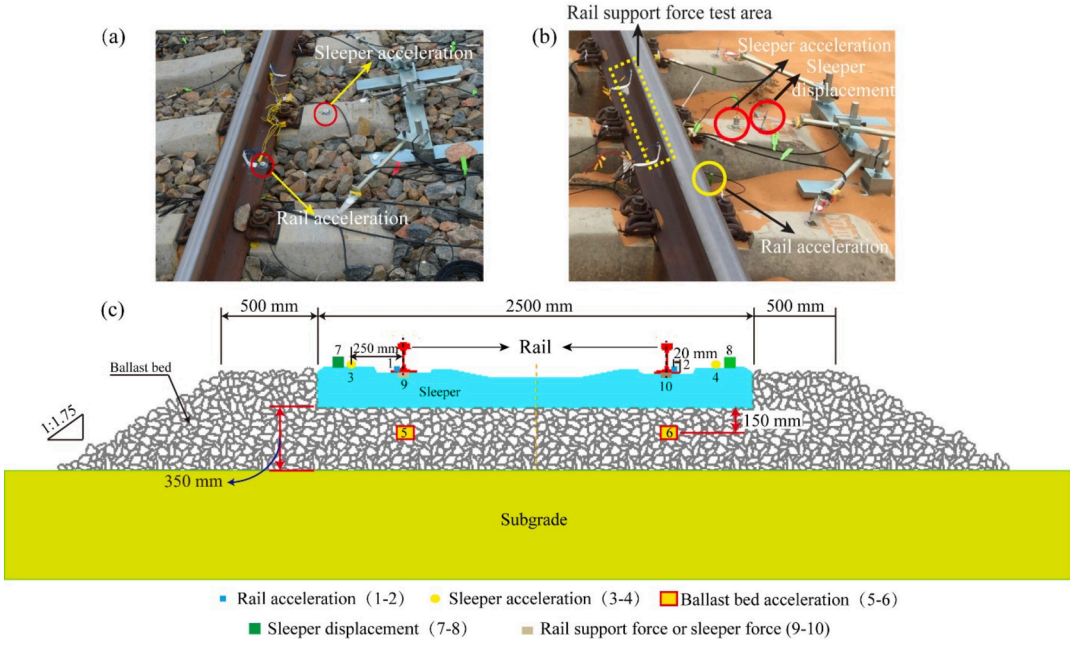

Fig. 6. Setup for vibration test: (a) clean section, (b) sandy section, (c) layout of measuring points.

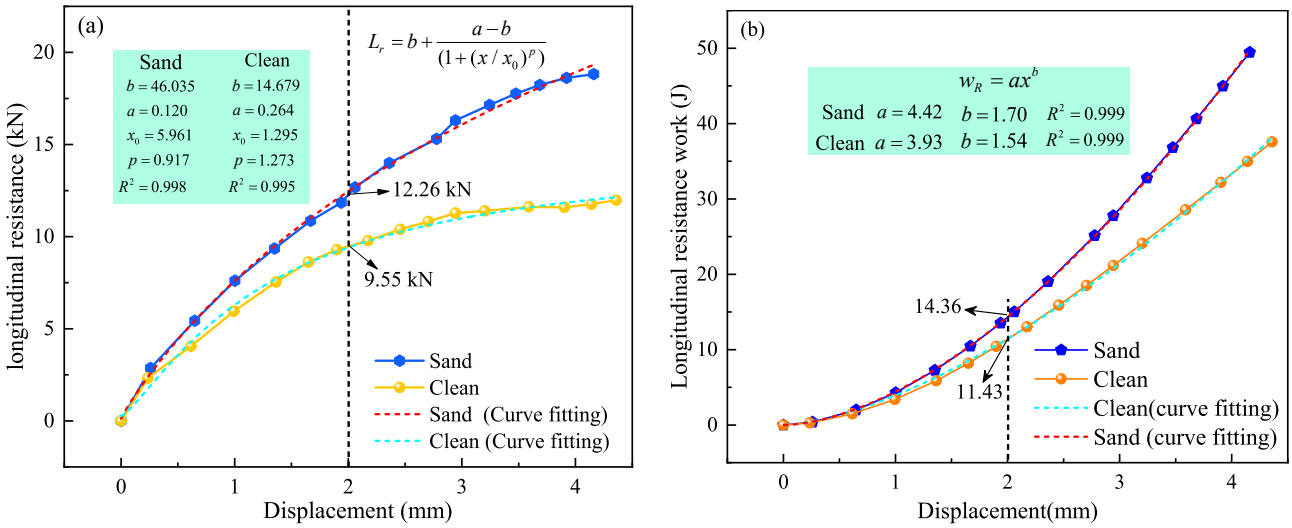

Fig. 7. Results of longitudinal resistance test: (a) Relationship between longitudinal resistance and displacement in sandy and clean sections, (b) Relationship between longitudinal resistance work and displacement in sandy and clean sections.

reference under the action of thrust.

In the processing phase, the displacements measured by the two dial indicators are first averaged. After that, the average displacement and longitudinal force measured at 5 different measuring points are collected, wherein the longitudinal force corresponding to 2 mm displacement is used as the indicator of the ballast bed longitudinal resistance [28,29]. The test setup is shown in Fig. 5.

2.2.2. Vibration test of track structure

The track vibration is one of the most important factors to access the performance of tracks and to determine the service life of tracks. During the sand intrusion, the voids in ballast beds are changed and thus the damping and vibration characteristics of ballast beds are also affected [23]. To study the effect of sand intrusion on the vibration behaviour of ballast beds, the acceleration tests of rails, sleepers, and ballast beds are measured under train loads in the sandy and clean sections respectively. The test setup is shown in Fig. 6.

The rail accelerometers are installed on the rail foot at 20 mm from the outer edge. The measurement range of rail accelerometers is up to 500 g and the precision is 5.03 mv/g. The sleeper accelerometers are installed on the top of the sleeper at 250 mm to the outer edge of the rails. The measurement range and precision of sleeper accelerometers are lower than that of rail accelerometers, which are 20 g and 248.8 mv/g respectively. The ballast accelerometers are installed 150 mm lower under the tested sleeper. The measurement range is 10 g, the precision is 503mv/g, and the frequency range is from 0.35 Hz to 5000 Hz. For the model validation in the next stage, the reaction force of the rail support and the dynamic displacement of the sleeper are also measured in the sandy section, as shown in Fig. 6 (b) and (c).

2.3. Results and analysis of the field test

2.3.1. Analysis of longitudinal resistance characteristics

The measurement results of the longitudinal resistance test are shown in Fig. 7, wherein the relationship between the longitudinal resistance force and displacement in Fig. 7 (a) and the relationship between the longitudinal resistance work and displacement in Fig. 7 (b).

As seen from Fig. 7 (a) that the longitudinal resistance of a single sleeper in the sandy section is 12.26 kN when the longitudinal displacement reaches 2 mm, while that in the clean section is 9.55 kN, indicating the sand intrusion leads to a 28.4% increase of the ballast bed longitudinal resistance. Besides, the slope of the two curves is also different. The longitudinal resistance grows slower after the displacement over 2 mm, showing the ballast bed resistance gradually converges. On the contrary, the slope of ballast bed resistance in the sandy section keeps at a higher value after 2 mm, which indicates the ballast bed resistance in the sandy section is expected to be much larger than that in the clean section. In order to better analyse the difference in the growth trend, the logistic regression analysis for the relationship between the longitudinal resistance and displacement is conducted. The fitting equation is as follows:

$$L_r = b + \frac{a-b}{(1+(x/x_0)^p)} \tag{1}$$

where L_r is the longitudinal resistance of the ballast bed, x is the longitudinal displacement of the sleeper, x_0 is first change point in the slope of the longitudinal resistance curve, a is the sum of the longitudinal contact force between the ballast particles (or sand particles) and the sleeper when the sleeper is not displaced, also referred to as the static longitudinal contact force of the sleeper, b is the limit of the longitudinal resistance of the ballast bed, showing the maximum capacity of the ballast bed to resist deformation.

Using Eq. (1), the static longitudinal contact force is 0.120 kN in the sandy section and 0.246 kN in the clean section. The static longitudinal contact force is reduced by 51.2% to the sand intrusion. This is because the contact between ballast particles and the sleeper in the sandy section is partly replaced by the contact between sand particles and the sleeper. Besides, the limit of the longitudinal resistance (predicted) of the sandy section is much larger than that of the clean section, which is 46.035 kN and 14.679 kN respectively. This is because sand particles fill the voids in the ballast bed, which largely increases the ballast bed longitudinal stiffness as well as the contact area between the sleeper bottom and the ballast bed. To further quantify the influence of sand intrusion on the longitudinal deformation resistance ability of single sleeper, the resistance work is used, following [30], as expressed in Eq. (2). The results are shown in Fig. 7 (b).

$$w_R = \int_0^x f(x)dx \tag{2}$$

where w_R is the longitudinal resistance work, x is the longitudinal displacement of the sleeper, and $f(x)$ is the expression of the resistance-displacement curve in Fig. 7 (a). Using Eq. (2), the longitudinal resistance work of the ballast bed in the sandy and clean sections are 14.36 J and 11.43 J, respectively, which is increased by 25.6%. This indicates that the sand intrusion can significantly increase the longitudinal

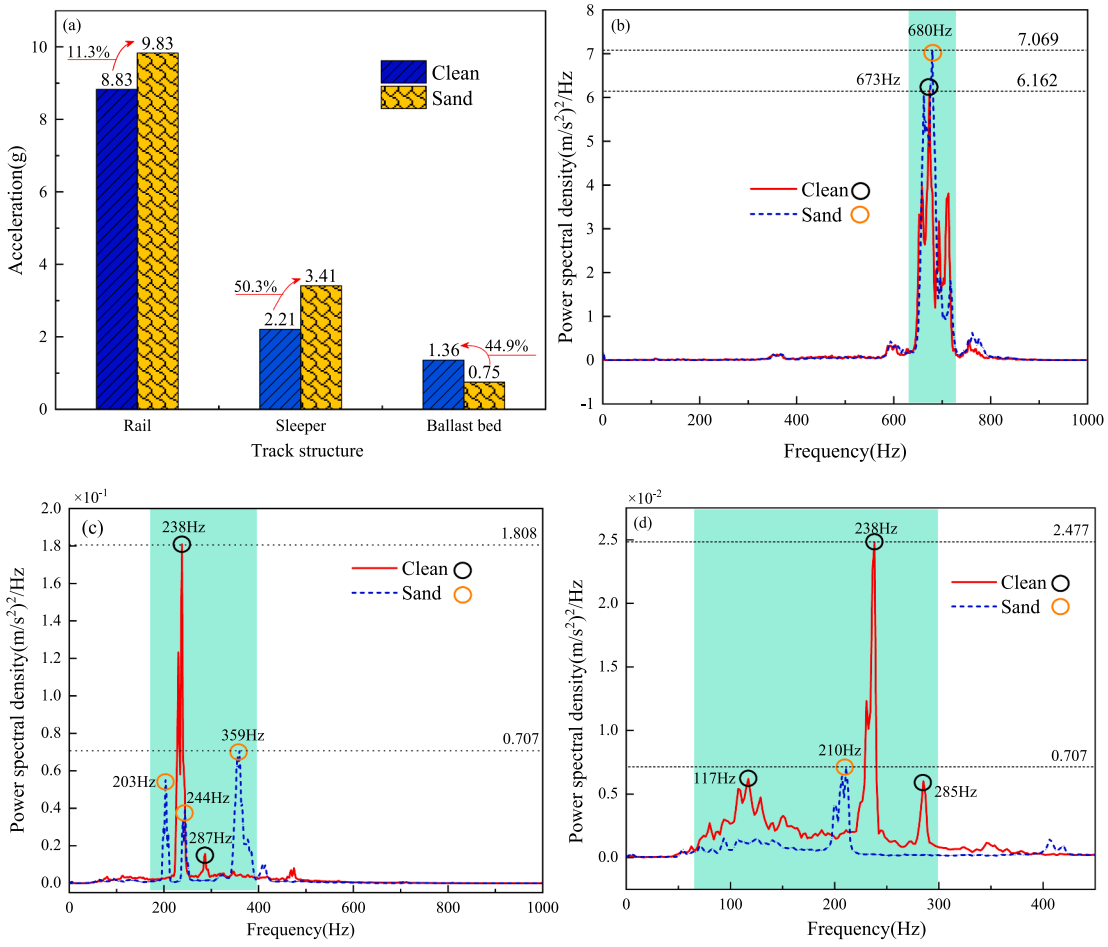

Fig. 8. Results of vibration test: (a) Acceleration of track components, (b) Power spectrum density of rails, (c) Power spectrum density of sleepers, (d) Power spectrum density of ballast beds.

resistance of the ballast bed, which match the findings of the analysis of the longitudinal resistance (see Fig. 7 (a)). The longitudinal resistance work is fitted by Eq. (3). The fitting coefficients a and b together reflect the increase in resistance work and the values are shown in Fig. 7 (b).

$$w_R = a_1 x^{b_1} \tag{3}$$

The fitting coefficients a_1 and b_1 in the sandy sections are larger than those in the clean section. This is because the sand intrusion changes the force chain in the ballast bed, which will be discussed in the next section.

2.3.2. *Vibration characteristics analysis of track structure*

The desert railway has been eroded by wind and sand all the year round. The continuous invasion of sand particles can certainly change the vibration level of track structure, affecting the usability and durability of track structure. The vibration acceleration amplitude (Time domain) and power spectral density (Frequency domain) of rail, sleeper and ballast bed in the sandy and clean sections are counted to explore the influence of sand intrusion on the vibration characteristics of track structure, as shown in Fig. 8.

It can be seen from Fig. 8 (a) that the rail and sleeper accelerations are increased by the sand intrusion, which is 11.3% and 50.3%, respectively, while the ballast acceleration is reduced by 44.9%. This can be explained by that the voids in the ballast bed are filled by sand particles and thus the stiffness of the ballast bed is increased. As a result, the vibration of rails and sleepers under train loads are amplified. However, the ballast particles become more restrained because the voids between ballast particles are no longer existed, which leads to a more integrated ballast bed and thus with less acceleration under train loads.

As seen from Fig. 8 (b), the main frequency band of the rail acceleration in the sandy section is 640–700 Hz and the highest energy appears at 680 Hz. The main frequency band of the rail acceleration in the clean section is 640–720 Hz and the highest energy appears 673 Hz, which is slightly changed. Different from the rail acceleration, the changes in the sleeper and ballast acceleration caused by the sand intrusion are much larger, as shown in Fig. 8 (c) and (d). The main frequency band of the sleeper acceleration is 220–240 Hz in the clean section and 200–400 Hz in the sandy section. The highest energy of sleeper acceleration appears at 238 Hz in the clean section and 359 Hz in the sandy section. The main frequency band of the ballast acceleration is changed from 100 to 300 Hz to 200–220 Hz by the sand intrusion and the highest energy from 283 Hz to 210 Hz. It shows that the sand intrusion significantly changes the energy distribution in the track. The frequencies of the highest energy of the rail and sleeper are increased while that of the ballast is decreased. In addition, it can be found that the single peak power spectral density of the maximum energy frequency of the sleeper and ballast bed of the sandy line is significantly smaller than that of the clean ballast bed, indicating that the sand intrusion has a great influence on the vibration frequency of the sleeper and ballast bed. Therefore, more attention should be paid to the long-term behaviour of the sleeper and ballast bed in sandy tracks.

3. Numerical analysis using discrete element modelling

3.1. *Model development*

The multi-scale effect is significant in sandy railway tracks, due to

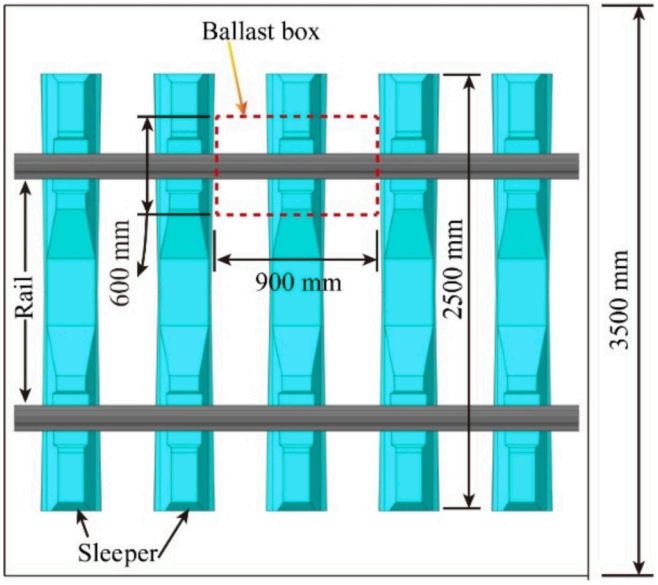

Fig. 9. Modelling area in track.

the large difference in particle size between ballast and sand particles [2]. The common problems in the modelling sandy track using the discrete element method are sand particles floating, difficulty to converge and high computational cost. To solve these problems, referring to previous studies [31,32], the ballast box model is used for simulation, as shown in Fig. 9. At the same time, in the modeling process, the sand particle size is enlarged by 5 times, and the average particle size is increased to 1.8 mm [10,33], which increases the self weight of a single sand particle. And the number of sand particles is reducedin the model according to the principle of mass conservation, so as to improve the efficiency and calculation speed of model balance. The sand particles are simulated by the ball units with a density of 2650 kg/m^3 and a particle size of 1.1 ~ 2.5 mm. Note that the actual size of sand particles is 0.22 ~ 0.5 mm.

The ballast bed is composed of ballast particles with distinct edges and different shapes [34]. It is crucial to consider the morphological characteristics of ballast particles in the discrete element model [35,36]. Therefore, the 3D laser scanning method is used to obtain the 3D profile of ballast particles which are imported into the discrete element software PFC 3D using a self-programmed Fish function. After that, ballast particles are generated by stacked spheres, as shown in Fig. 10 (a) and (b).

According to the actual situation of the sandy track, the thickness of the ballast bed is set as 0.35 m and the standard gradation curve is adopted (the red line in Fig. 3 (a)). The sleeper is modelled according to the new type II concrete sleeper in China. Because the force from the sleeper mainly concentrates under the rail, the area of 300 mm on both sides of the rail center line (in total 600 mm) is considered to avoid the problem that the model is difficult to converge and the boundary effect. The sleeper is modelled using ball units (see Fig. 10 (c)) and in this way, the detailed dimension of the sleeper can be achieved. Finally, the ballast bed model and the sleeper model are spliced together to generate a sleeper-sandy ballast bed discrete element model, as shown in Fig. 10 (d).

3.2. Contact model between particles

The previous studies [37,38,40] have shown that the linear contact model can reduce the calculation cost, improve the calculation efficiency, and the results are reliable. Because the railways in sandy regions are mostly dry and the dry sand particles and ballast particles are non-sticky materials, the linear contact model between particles is used to improve the computation efficiency. The contact in the sleeper-sandy ballast bed model includes the sand-sand contact, the ballast-ballast contact, the sand-ballast contact, the sand-sleeper contact, and the ballast-sleeper contact. There are many types of contact materials in the model, and the calculation process is complicated. However, it can be seen from the modeling process in Section 3.1 that sand particles, ballast particles, and the sleeper are all generated by stacked spheres. Therefore, it is important to carefully consider the contact form and overlap

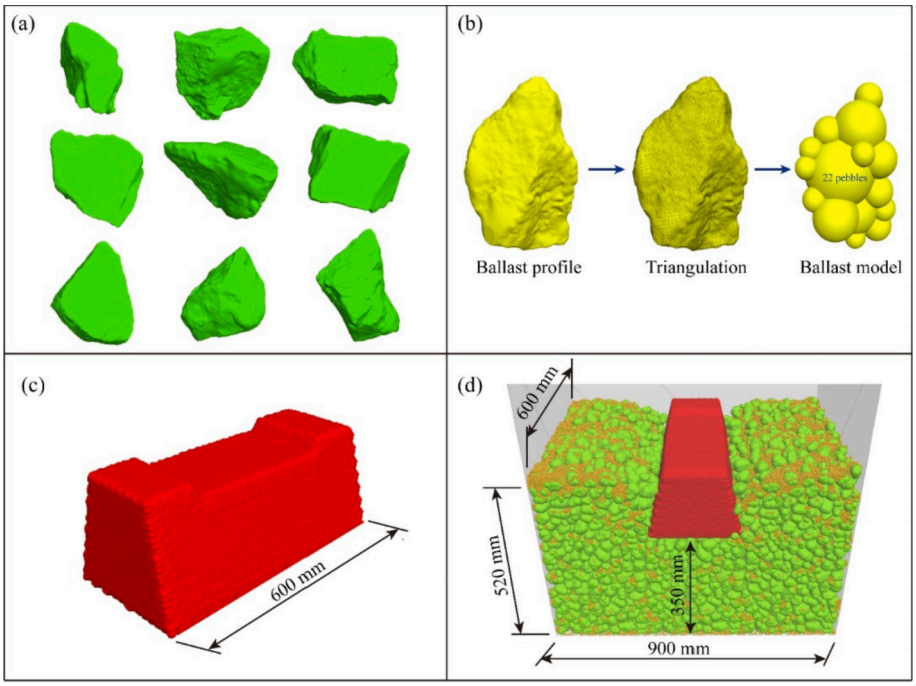

Fig. 10. Development of discrete element model: (a) Scanned profile of ballast particles, (b) Generation of a ballast particle, (c) Sleeper model, (d) Overview of ballast box model.

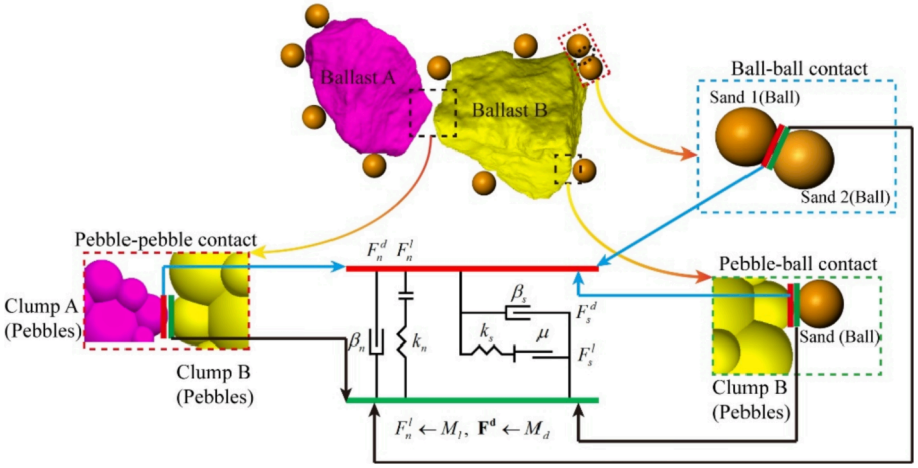

Fig. 11. Contact model between particles.

between spheres, as shown in Fig. 11.

As seen from Fig. 11, the contact in the sleeper-sandy ballast bed model can be divided into the contact between the same material (i.e., sand-sand or ballast-ballast) and the contact between different materials (i.e., sand-ballast, sand-sleeper, and ballast-sleeper), which are discussed respectively.

(1) The same material

The linear contact model is used to calculate the contact force of the same particle material. The contact force is first decomposed into normal contact force and tangential contact force and then calculated [37], as shown in Eqs. (4)–(9).

$$F_n = F_n^l + F_n^d, \tag{4}$$

$$F_n^l = k_n x_n, \tag{5}$$

$$F_n^d = c_n \dot{x}_n, \tag{6}$$

$$F_s = F_s^l + F_s^d, \tag{7}$$

$$F_s^l = k_s x_s, \tag{8}$$

$$F_s^d = c_s \dot{x}_s, \tag{9}$$

where F_n is the normal contact force, F_n^l is the normal spring force, F_n^d is the normal damping force, x_n is the overlap between particles in the normal direction, k_n is the normal contact stiffness. c_n is the normal damping coefficient, $\dot{x}_n$ is the normal relative velocity, F_s is the tangential contact force, F_s^l is the tangential spring contact force, F_s^d is the tangential damping force, x_s is the tangential relative displacement, k_s is the tangential contact stiffness, c_s is the tangential damping coefficient, $\dot{x}_s$ is the tangential relative velocity. The damping coefficient c_n and c_s can be calculated by Eqs. (10) and (11). The slip between particles can be determined by the Mohr-Coulomb criterion.

$$c_n = (2\beta_n \sqrt{m_c k_n}) \tag{10}$$

$$c_s = (2\beta_s \sqrt{m_c k_s}) \tag{11}$$

where β_n and β_s are the normal critical damping ratio and tangential critical damping ratio, respectively. m_c is the effective inertial mass, which can be calculated by Eq. (12).

$$m_c = \frac{m_1 m_2}{m_1 + m_2} \tag{12}$$

Table 1
Contact parameters used in discrete element model.

Parameter	Value
Density of ballast/(kg/m^3)	2600
Density of sand particle/(kg/m^3)	2650
Density of sleeper/(kg/m^3)	2500
Normal contact stiffness of ballast/(N/m)	4.5×10^7
Tangential contact stiffness of ballast/(N/m)	3.5×10^7
Friction coefficient of ballast particle	0.5
Normal contact stiffness of sand particle/(N/m)	2.0×10^5
Tangential contact stiffness of sand particle/(N/m)	1.5×10^5
Friction coefficient of sand particle	0.4
Normal contact stiffness of sleeper/(N/m)	4.0×10^7
Tangential contact stiffness of sleeper/(N/m)	3.0×10^7
Friction coefficient of sleeper	0.5

where m_1 is the mass of particle 1, e.g., Sand 1 in Fig. 11. m_2 is the mass of particle 2, e.g., Sand 2 in Fig. 11.

(2) Different materials

The calculation of the contact force between different granular materials is similar to that between the same granular materials. The difference is that the normal contact stiffness, tangential contact stiffness and friction coefficient should be transformed according to the principle of attribute inheritance [37], as shown in Eqs. (13)–(15).

$$\frac{1}{k_n} = \frac{1}{k_n^a} + \frac{1}{k_n^b}, \tag{13}$$

$$\frac{1}{k_s} = \frac{1}{k_s^a} + \frac{1}{k_s^b}, \tag{14}$$

$$\mu = \min(\mu_a + \mu_b), \tag{15}$$

where k_n^a and k_n^b are the normal contact stiffness of material a and b, respectively. k_s^a and k_s^b are the tangential contact stiffness of material a and b, respectively. μ_a and μ_b are the friction coefficients of material a and b, respectively.

The contact parameters between the sleeper, sand particles, and ballast particles used in the model are adopted from references [2,4,33,38–40], as shown in Table 1.

3.3. Model validation

To verify the model of sleeper-sandy ballast bed model, the actual

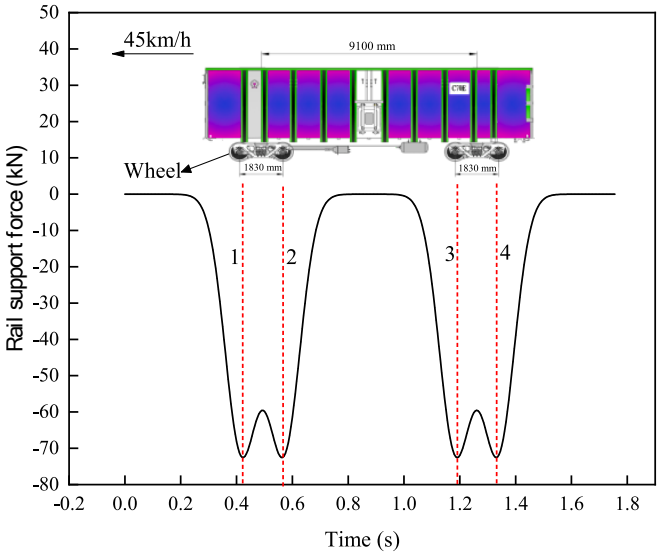

Fig. 12. Train load fitted from measured rail support force.

train load is used as input and the dynamic displacement of the sleeper and acceleration of the ballast bed are calculated. The train load is fitted from the measurement results of rail support force (described in Section 2.3) using Eq. (16) [2,4,41,42]. The train load is shown in Fig. 12.

$$F(t) = p \times a_2 \times \sum_{i=1}^{2} e^{\frac{-(vt-x_i)^2}{2*b_2^2}} \tag{16}$$

where $F(t)$ is the rail support force at time t, p is the static wheel load, which is 115 kN. a_2 is the static wheel load reduction coefficient, which is 0.45. b_2 is the longitudinal influence range of a single wheel load, which is 0.6. v is the train speed, which is 45 km/h according to the field measurement. x_i is the longitudinal position of the i-th wheel.

Using the train load as input to the sleeper-sandy ballast bed model, the calculation results of the amplitude dynamic displacement of the sleeper and the amplitude acceleration of the ballast bed are compared with the measurement results, which is shown in Fig. 13.

As seen from Fig. 13 (a), the average of the amplitude dynamic displacement of the sleeper of the measurement is 0.324 mm and that of the simulation is 0.333 mm. The difference is very small, which is only 2.9 %. Similarly, Fig. 13 (b) shows the average of the amplitude acceleration of the ballast bed from measurement and simulation results are close, which are 0.75 g and 0.72 g, respectively. Therefore, simulation and measurement results match well, indicating the sleeper-sandy ballast bed model can simulate the dynamic behaviour of sandy railway track correctly and can be used for further analysis.

4. Simulation results and parametric study

The train speed and axle load are the most important factors to determine the stress state of railway tracks. The effect of the sand intrusion can also be different under various train speeds and axle loads. Thus, 9 operating conditions of sandy tracks with different train speeds and axle loads are analyzed in this section. The detailed simulation cases are shown in Table 2.

4.1. Effect of train speed

The invasion and deposition of sand particles can change the working performance of ballast bed under different operating speeds and affect the safety of line operation. The effect of sand intrusion on sandy track under various train speeds is analysed in this section. The contact force chain in the sandy track during train passing under various train speeds (Case V1 to V4) is shown in Fig. 14.

As seen from Fig. 14, the contact force chains are distributed in a frustum shape in all cases and gradually become sparse vertically downwards along the ballast bed. Besides, the areas where the weak contact force chains appear, e.g., Area a and Area b (see Fig. 14), become more intensively distributed as the train speed increases, however, with a small change which is up to 38 N and thus barely affects overall distribution. This shows that the increase of train speed has little effect on the force state in the ballast bed.

Table 2
Simulation cases.

Case Name		Axle load (t)	Speed (km/h)
Cases with different train speeds	V1	23	45
	V2		60
	V3		90
	V4		120
Cases with different axle loads	W1	21	60
	W2	23	
	W3	25	
	W4	27	
	W5	30	

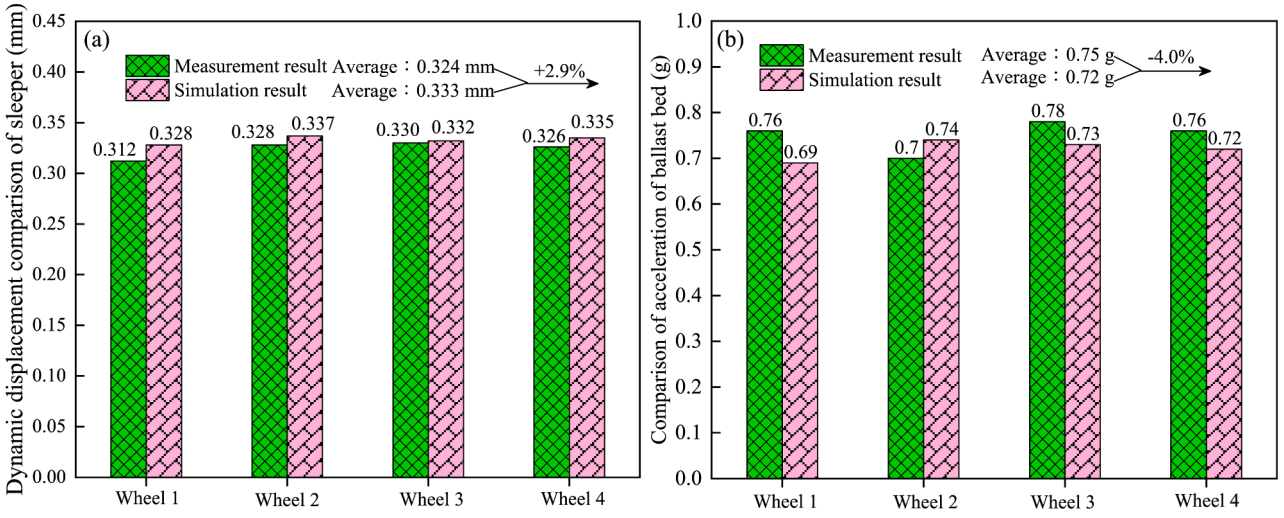

Fig. 13. Comparison between simulation and measurement results: (a) Amplitude dynamic displacement of sleeper, (b) Amplitude acceleration of ballast bed.

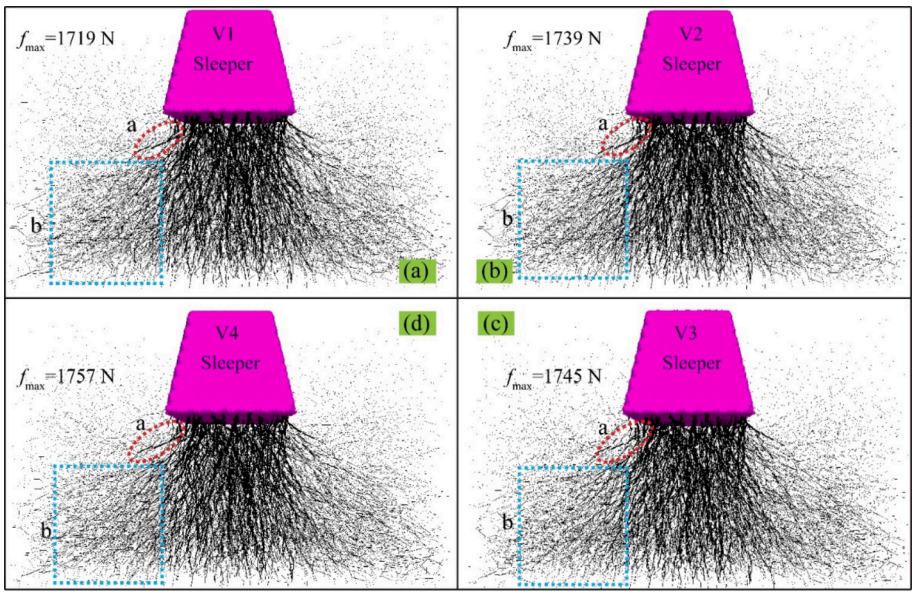

Fig. 14. Contact force chains in sandy ballast bed under various train speeds: (a) 45 km/h, Case V1, (b) 60 km/h, Case V2, (c) 90 km/h, Case V3, (d) 120 km/h, Case V4.

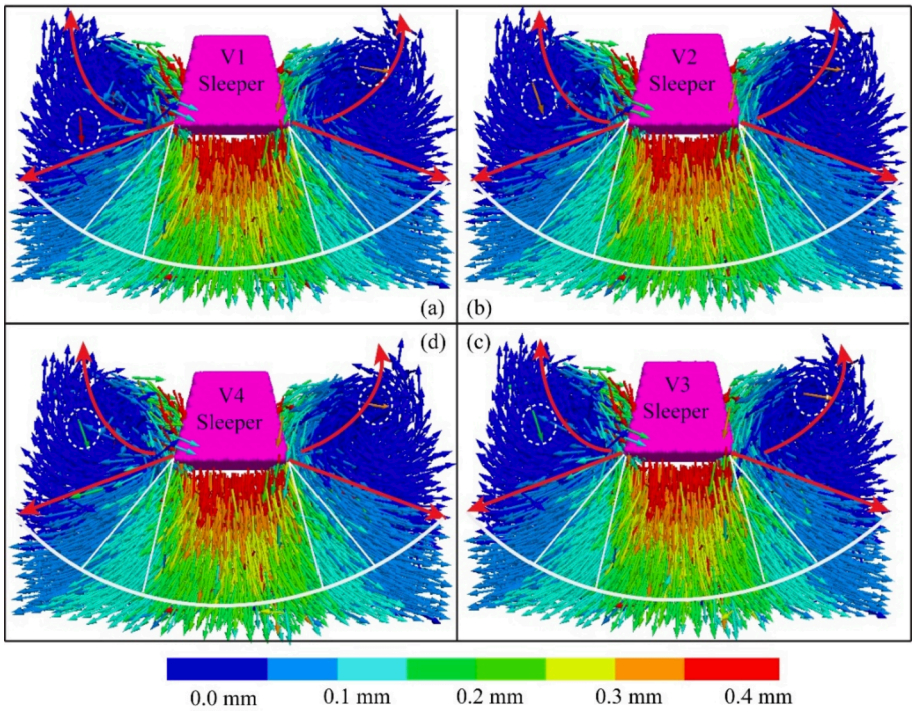

Fig. 15. Particle displacements in sandy ballast bed under various train speeds: (a) 45 km/h, Case V1, (b) 60 km/h, Case V2, (c) 90 km/h, Case V3, (d) 120 km/h, Case V4.

The displacement and direction of ballast particles directly affect ballast settlement, which plays an important role in determining track smoothness [44]. To study the effect of train speeds on the displacement of ballast particles in sandy ballast bed, the distribution of the displacement of ballast particles during train passing is collected using a self-programmed Fish function as shown in Fig. 15. The colours in the Fig. 15 indicate the amplitude of displacement and the arrows the direction.

It can be seen from Fig. 15 that under the peak train load, the ballast particles at the bottom of the sleeper move radially downwards. On the contrary, the ballast particles at the sides of the sleeper move upward in an arc trajectory and the displacement gradually reduces in the lower part. As the train speed increase, the displacements of the ballast particle at the sides of the sleeper reduce slightly and that at other parts in the track remains stable. This shows that within a certain speed range, the increase of the train speed can not change the overall movement trend of the ballast particles in sandy ballast bed. The reason is that the sand particles envelop the ballast particles and restrict the movement of the ballast particles. The dynamic load transmitted by the train speed growth is not enough to overcome the restraint of the sand particles on the ballast. As a result, the overall distribution of ballast particles displacement does not change with the train speed.

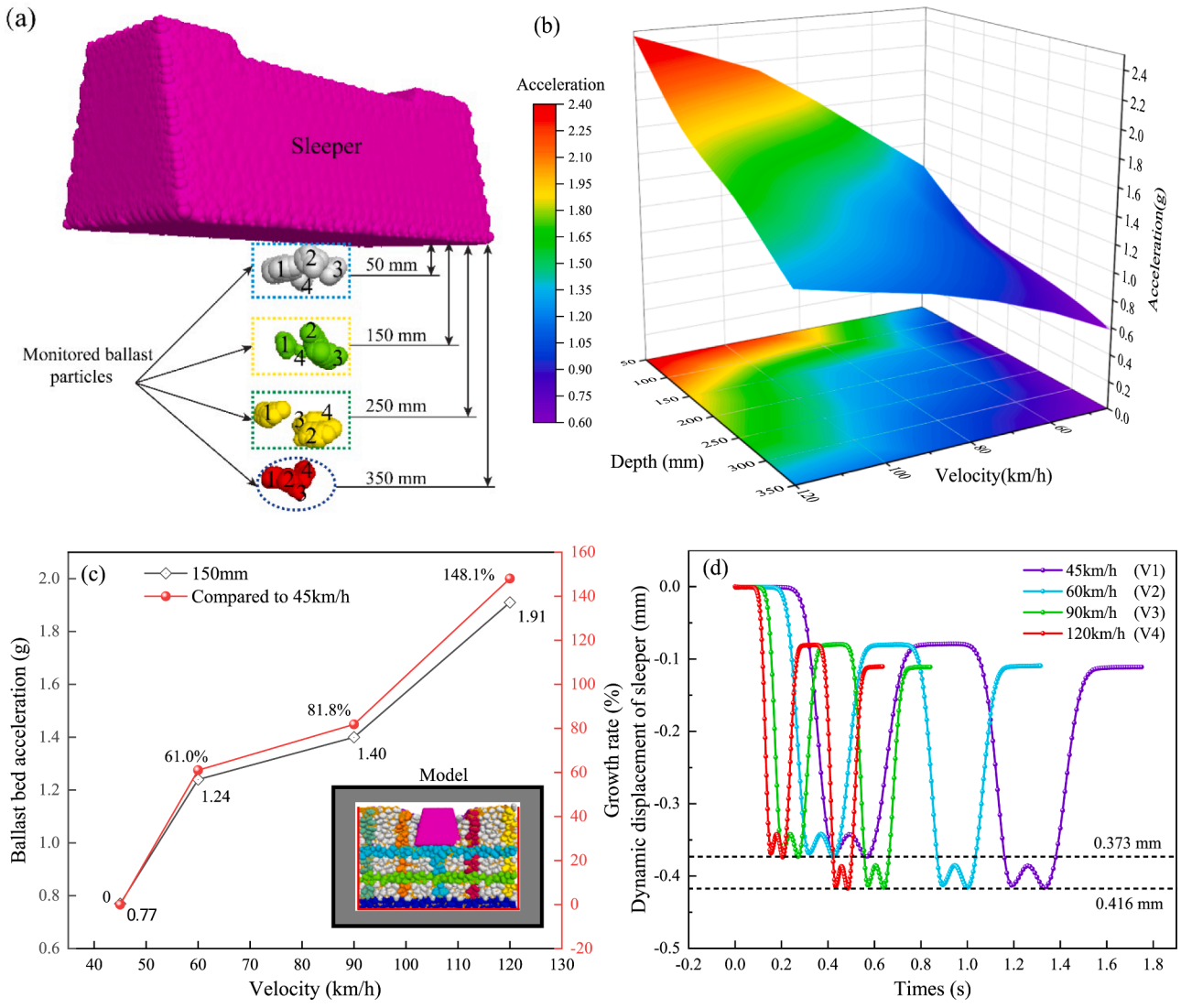

Fig. 16. Acceleration under various train speeds: (a) Ballast bed acceleration monitoring position, (b) Average acceleration of ballast particles, (c) Overall acceleration of ballast bed, (d) Dynamic displacement of sleeper.

To further study the effect of train speeds, the acceleration of four ballast particles at four positions under the sleeper is tracked during train passing (in total 16 particles), which are the particles at 50 mm, 150 mm, 250 mm, and 350 mm below the sleeper bottom respectively, as shown in Fig. 16 (a). The average acceleration of the ballast particles at different positions in the ballast bed under various train speeds is shown in Fig. 16 (b). Using the average acceleration of the ballast particles at 150 mm below the sleeper for the overall acceleration of the ballast bed, the overall acceleration of the ballast bed under various train speeds is compared in Fig. 16 (c). The dynamic displacement of the sleeper under various train speeds is compared in Fig. 16 (d).

As seen from Fig. 16 (b), the acceleration of ballast particles gradually reduces downwards along the vertical direction while the acceleration of ballast particles at all positions increases as the train speed grows. Similarly, the overall acceleration of the ballast bed also increases by the train speed, as seen from Fig. 16 (c), which is 0.77 g, 1.24 g, 1.40 g, and 1.91 g at Case V1-V4, respectively. It is remarkable to note that the overall acceleration of the ballast bed increased by approximately 148.1% when the train speed grows from 45 km/h to 120 km/h. This indicates that the increase of train speed in sandy ballast bed can significantly lead to the amplification of ballast bed vibration.

It can be seen from Fig. 16 (d) that the maximum sleeper displacement does not change under different train speeds. It indicates the train speed has little effect on the elastoplastic deformation of the ballast bed, which matches the findings of the microscopic displacements of ballast particles. Besides, it also shows the correlation between the sleeper displacement and ballast bed acceleration is weak.

4.2. *Effect of axle load*

The axle load of trains directly determines the force state of railway tracks. Trains with high axle loads aggravate ballast pulverization and thus reduce the service life of ballast beds. Studies [43,45] have shown the mesoscopic movement of ballast particles is an effective means to indicate the macroscopic behaviour of the ballast bed. Similar to Section 4.1, the contact force chain in the ballast bed and the displacement of ballast particles under various axle loads, i.e., Case W1-W5, are shown in Fig. 17.

It can be seen from Fig. 17 (a)–(e) that as the axle load increases, the distribution of contact force chains becomes more intensive, more ballast particles join in the network of chains and the diffusion angle of the distribution gradually increases from 45° to 57°. Moreover, the maximum contact force also increases along with the axle load, which is 2317 N in Case W5 and 1604 N in Case W1, increased by 44.5%. It indicates the axle loads closely correlates to contact forces between particles in sandy ballast bed.

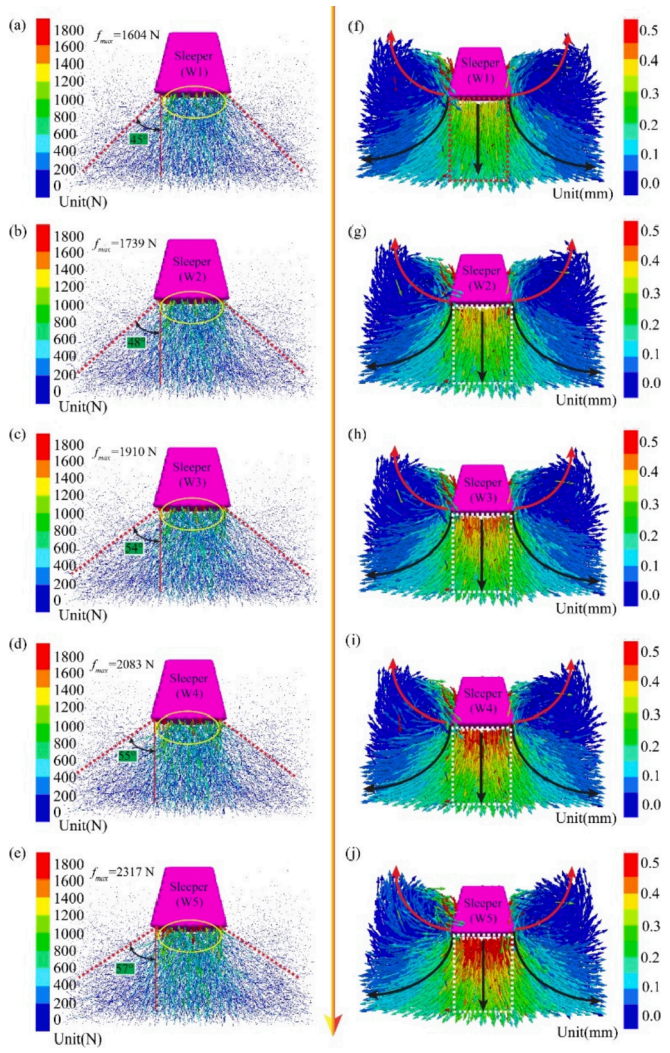

Fig. 17. Contact force chains and ballast particle displacements under various axle loads: (a) & (f) 21 t, Case W1, (b) & (g) 23 t, Case W2, (c) & (h) 25 t, Case W3, (d) & (i) 27 t, Case W4, (e) & (j) 30 t, Case W5.

Fig. 17 (f)–(j) shows that the displacements of ballast particles under the sleepers are increased as the axle load grows, which can be seen by the amounts of the red arrows under the sleeper. It indicates the axle load has a large influence on the displacements of the ballast particles by changing the distribution of ballast particles, which reflects in the macroscopical aspect as dynamic displacement of sleeper and track settlement.

Similar to Section 4.1, the average acceleration of the ballast particles at different positions in the ballast bed and the overall acceleration of the ballast bed under various axle loads are shown in Fig. 18.

It can be seen from Fig. 18 (a) that as the axle load grows, the acceleration of ballast particles at all positions all increases. The ballast particles close to the sleeper bottom shows a larger increase than that at a deeper position. Fig. 18 (b) shows that the overall acceleration of the ballast bed increases along with the axle load. The overall acceleration increases from 1.19 g to 1.50 g when the axle load grows from 21 t to 25 t, increasing by 25.7%. It indicates the axle loads has a large effect on the ballast acceleration in sandy ballast bed, with a positive correlation.

From the aspect of the growth rate of the overall acceleration, the growth is small in the first and last phases, while large in the middle phase (corresponding to the increase from 23 t to 25 t). 23 t is the inflection point of the growth rate. The reason is that the restraint effect of sand particles on ballast particles is weakened by the large axle load, leading to the increase in both unbalanced forces and particle displacements. As a result, the vibration of ballast particles becomes larger, which match the changes in the displacements of ballast particles discussed in Fig. 17.

To further study the effect of the axle load on the dynamic characteristics of sandy tracks, the dynamic displacement of the sleeper and the elastic strain energy per unit axle load under different axle loads are compared, as shown in Fig. 19. Note that the elastic strain energy per unit axle load refers to the ratio of elastic strain energy of the ballast bed to the axle load of the train that passing the track, which is commonly used to compare the effect of different trains on the elastic deformation of ballast beds, as shown in Eq. (17).

$$w(T) = \frac{W_f(T)}{M_T}, \tag{17}$$

where $w(T)$ is the elastic strain energy per unit axle load (J/t), $W_f(T)$ is the elastic strain energy of the ballast bed during the train passing (J), M_T is the axle load (t), and T is the action time of train load (s).

It can be seen from Fig. 19 that as the axle load grows, the dynamic displacement of the sleeper and the elastic strain energy per unit axle load gradually increase, indicating that they are sensitive to the change of axle loads, which match the mesoscopic results of displacements of ballast particles (see Fig. 17). To characterize the effect of axle load more accurately, the maximum displacement of the sleeper, maximum elastic deformation of ballast bed, maximum plastic deformation of ballast bed,

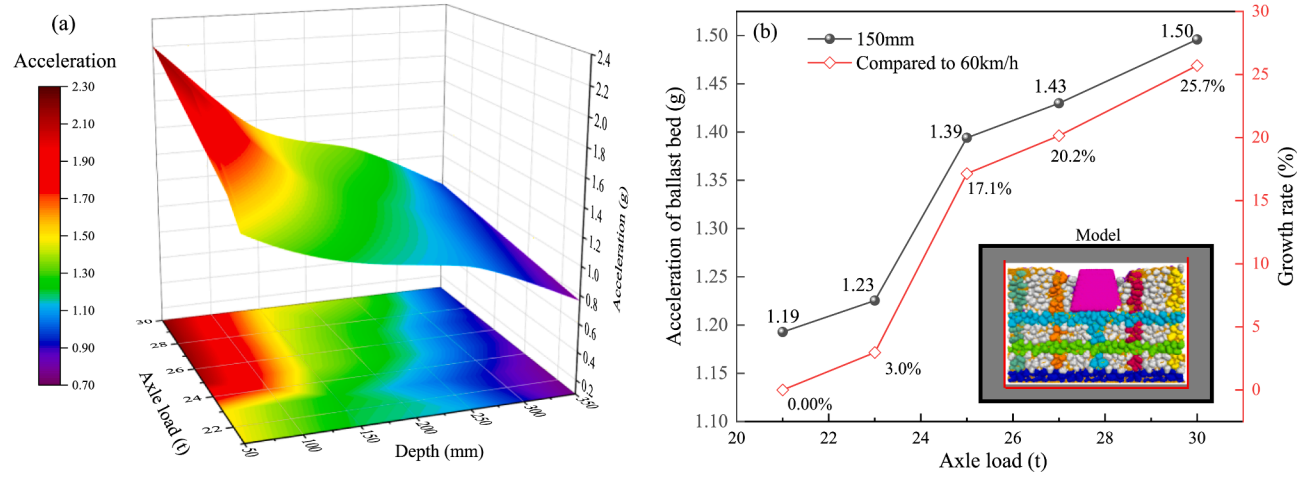

Fig. 18. Acceleration under various axle loads: (a) Average acceleration of ballast particles, (b) Overall acceleration of ballast bed.

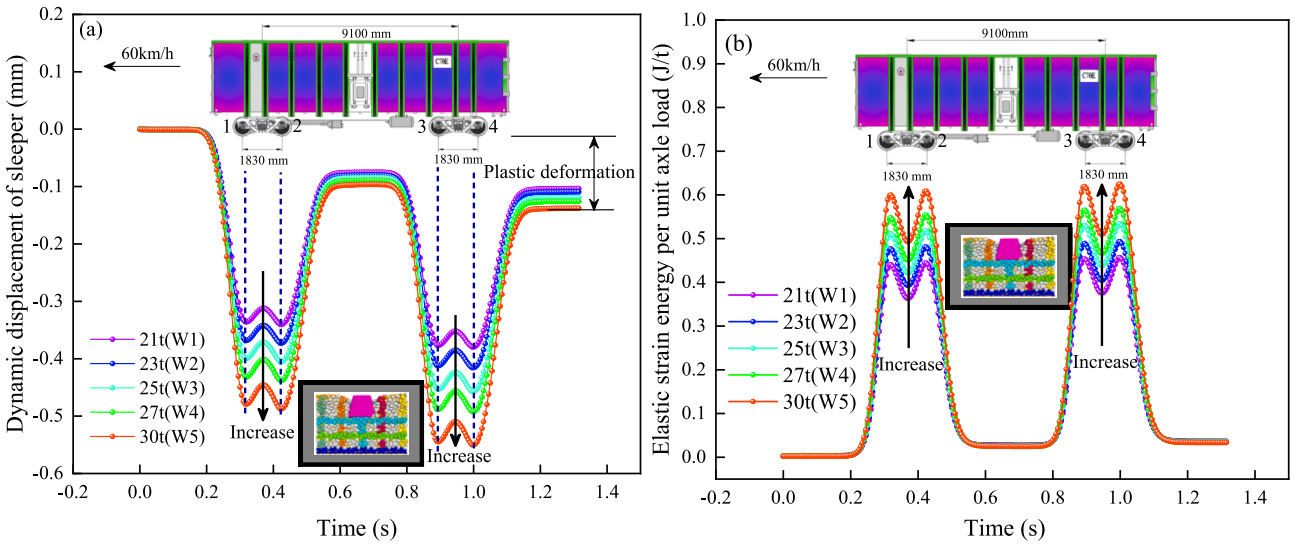

Fig. 19. The variation law of dynamic displacement and strain energy of sleeper under different axle loads: (a) Dynamic displacement of sleeper, (b) Elastic strain energy per unit axle load.

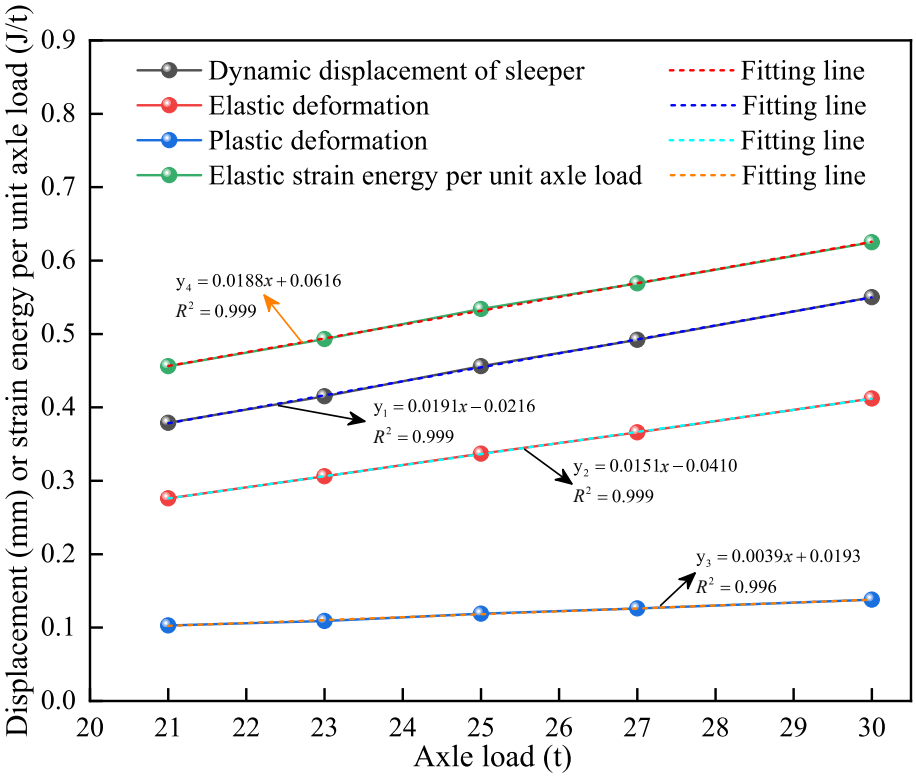

Fig. 20. Comparison between sleeper displacement, ballast bed deformation, and elastic strain energy.

and the maximum elastic strain energy per unit axle load are fitted using linear functions and compared in Fig. 20.

It can be seen from Fig. 20 that the slope of the sleeper displacement is the largest (0.0191), that of the elastic strain energy per unit axle load the second (0.0188), that of the elastic deformation of the ballast bed the third (0.0151), and that of the plastic deformation of the ballast bed the smallest (0.0039). This indicates as the axle load grows, the plastic deformation of the ballast bed increases at a slower pace while the elastic deformation increases faster. Therefore, sandy ballast bed have the potential to operate trains with large axel loads from the aspect of ballast deformation. However, further studies should be conducted to explore the adaptability of sleepers and rails in sandy tracks under large axel loads.

5. Conclusions

The sand intrusion in railway tracks in sandy regions can significantly change the mechanical behaviour of tracks and thus threaten the safety of train operation. Aiming at the deficiencies of existing experimental and numerical research, this paper presents substantial field tests on both sandy and clean railway tracks to study the effect of sand intrusion on the longitudinal resistance of track beds and the vibration

behaviour of track structures. After that, a 3D multi-scale sleeper-sandy ballast bed model using the discrete element method is developed to study the micro-contact between ballast particles and the vibration behaviour of sandy ballast bed under various train speeds and axle loads. The following conclusions have been found.

(1) The ballast bed longitudinal resistance test shows that the longitudinal resistance of a single sleeper in the clean ballast bed is 9.55 kN, while that in the sandy ballast is 12.26 kN, increased by 28.4%. This is because sand particles fill the voids in the ballast bed, which largely increases the ballast bed longitudinal stiffness as well as the contact area between the sleeper bottom and the ballast bed. Besides, the longitudinal resistance work of the ballast bed in the clean and sandy ballast bed are 11.43 J and 14.36 J, respectively, with a 25.6% difference, indicating that the sand intrusion can improve the longitudinal resistance of ballast beds.
(2) The track vibration test shows the rail and sleeper accelerations are increased by the sand intrusion, which is 11.3% and 50.3%, respectively, while the ballast acceleration is reduced by 44.9%. Besides, sand intrusion significantly changes the energy distribution in the track. The frequencies of the highest energy of the rail and sleeper are increased while that of the ballast bed is decreased. Besides, it can be found the effect of the sand intrusion on the sleeper and ballast bed is quite large compared to that on the rail. Therefore, more attention should be paid to the long-term behaviour of the sleeper and ballast in sandy tracks.
(3) Numerical analysis shows that the growth of train speed has little effect on the force state and particle movement in the ballast bed and sleeper displacement, while the large effect on the ballast acceleration. The overall acceleration of the ballast bed increased by approximately 148% when the train speed grows from 45 km/h to 120 km/h.
(4) The growth of axle load has a significant influence on the mechanical behaviour of sandy ballast bed. As the axle load increases, the diffusion angle of the distribution of contact force chains gradually increases from 45° to 57° and the maximum contact force between ballast particles increase from 1604 N to 2317 N, increasing by approximately 45%. The displacements of ballast particles under the sleepers are increased as the axle load grows, indicating the axle load has a large influence on the contact characteristics of ballast particles.
(5) As the axle load grows, the sleeper displacement, ballast deformation, and the elastic strain energy per unit axle load show a trend of linear growth. The growth rate of the sleeper displacement is the largest, followed by the elastic strain energy per unit axle load and the elastic deformation of the ballast bed, while the growth rate of the plastic deformation of the ballast bed is the smallest. It indicates that sandy tracks have the potential to operate trains with large axel loads from the aspect of ballast deformation. However, further studies should be conducted to explore the adaptability of sleepers and rails in sandy tracks under large axel loads.

CRediT authorship contribution statement

Hong Xiao: Project administration, Funding acquisition, Supervision. **Zhihai Zhang:** Conceptualization, Methodology, Formal analysis, Writing – original draft. **Yihao Chi:** Software, Validation, Formal analysis. **Xiaoyu Wang:** Software, Data curation. **Haoyu Wang:** Writing – review & editing. **Ziqing Jiang:** Software.

Declaration of Competing Interest

The authors declare that they have no known competing financial interests or personal relationships that could have appeared to influence the work reported in this paper.

Acknowledgments

This work was supported by the National Natural Science Foundation of China (Grant number 51978045) and the Fundamental Research Funds for the Central Universities (Grant number 2021YJS128).

References

[1] E.T. Selig, J.M. Waters, Track geotechnology and substructure management, Thomas Telford, London, 1994.
[2] H. Xiao, Z.H. Zhang, X.H. Cui, F. Jin, Experimental study and discrete element analysis of ballast bed with various sand content, Constr. Build. Mater. 271 (2021), 121869.
[3] L.L. Fu, S.H. Zhou, P.J. Guo, Z.K. Tian, Y.X. Zheng, Dynamic characteristics of multiscale longitudinal stress and particle rotation in ballast track under vertical cyclic loads, Acta Geotech. 16 (2021) 1527–1545.
[4] Z.H. Zhang, H. Xiao, M. Wang, G.P. Liu, H.Y. Wang, Mechanical behavior and deformation mechanism of ballast bed with various fouling materials, J. Central South Univ. 27 (10) (2021) 1–18.
[5] N.T. Ngo, B. Indraratna, C. Rujikiatkamjorn, DEM simulation of the behaviour of geogrid stabilised ballast fouled with coal, Comput. Geotech. 55 (2014) 224–231.
[6] N.T. Ngo, B. Indraratna, C. Rujikiatkamjorn, Modelling geogrid-reinforced railway ballast using the discrete element method, Transp. Geotech. (2016) 86–102.
[7] H. Huang, E. Tutumluer, Discrete Element Modeling for fouled railroad ballast, Constr. Build. Mater. 25 (8) (2011) 3306–3312.
[8] E. Tutumluer, W. Dombrow, H. Huang, Laboratory characterization of coal dust fouled ballast behaviour, in: C. Nashville (Ed.), AREMA 2008 Annual Conference and Exposition September. 21-24, 2008.
[9] L. Bruno, M. Horvat, L. Raffaele, Windblown sand along railway infrastructures: A review of challenges and mitigation measures, J. Wind Eng. Ind. Aerodyn. 177 (2018) 340–365.
[10] Z.H. Zhang, H. Xiao, M. Wang, M.Y. Zhang, J.Q. Wang, Research on dynamic mechanical behavior of ballast bed in windblown sand railway based on dimensional analysis, Constr. Build. Mater. 287 (2021), 123052.
[11] J. Sadeghi, A.R. Tolou Kian, H. Ghiasinejad, M.F. Moqaddam, S. Motevalli, Effectiveness of geogrid reinforcement in improvement of mechanical behavior of sand-contaminated ballast, J. Geotextiles Geomembranes 48 (2020) 768–779.
[12] J. Sadeghi, A.R. Tolou Kian, M. Fallah, Experimental Investigation of Mechanical Properties of Ballast Contaminated with Wet Sand Materials, Int. J. Geomech. 21 (1) (2021) 04020241.
[13] D. Akbar, P. Massoud, M.A. Asghar, Effect of sand and clay fouling on the shear strength of railway ballast for different ballast gradations, Granular Matter. 20 (51) (2018) 1–14.
[14] A.R. Tolou Kian, J. Sadeghi, J.A. Zakeri, Large-scale direct shear tests on sand-contaminated ballast, Proc. Inst. Civil Eng.-Geotech. Eng. 171 (5) (2018) 451–461.
[15] A.R. Tolou Kian, J.A. Zakeri, J. Sadeghi, Experimental investigation of effects of sand contamination on strain modulus of railway ballast, J. Geomech. Eng. 14 (6) (2018) 563–570.
[16] A.R. Tolou Kian, J. Sadeghi, J.A. Zakeri, Influences of railway ballast sand contamination on loading pattern of pre-stressed concrete sleeper, Constr. Build. Mater. 233 (2020), 117324.
[17] J.A. Zakeri, R. Abbasi, Field investigation of variation of loading pattern of concrete sleeper due to ballast sandy contamination in sandy desert areas, J. Mech. Sci. Technol. 26 (12) (2012) 3885–3892.
[18] J.A. Zakeri, M. Esmaeili, M. Fathali, Evaluation of humped slab track performance in desert railways, Proc. Inst. Mech. Eng. Part F 225 (6) (2011) 566–573.
[19] M. Koohmishi, M. Palassi, Effect of gradation of aggregate and size of fouling materials on hydraulic conductivity of sand-fouled railway ballast, Constr. Build. Mater. 167 (2018) 514–523.
[20] M. Esmaeili, J.A. Zakeri, S.A. Mosayebi, Effect of sand-fouled ballast on train-induced vibration, Int. J. Pavement Eng. 15 (7) (2014) 635–644.
[21] M. Esmaeili, P. Aela, A. Hosseini, Experimental assessment of cyclic behavior of sand-fouled ballast mixed with tire derived aggregates, Soil Dyn. Earthq. Eng. 98 (2017) 1–11.
[22] M. Esmaeili, P. Aela, A. Hosseini, Effect of moisture on performance of mixture of sand-fouled ballast and tire-derived aggregates under cyclic loading, J. Mater. Civil Eng. 31 (2) (2019) 04018377.
[23] W.R. Tyfour, Effect of moving sand as a ballast contaminant on rail corrugation: field experience, Int. J. Environ. Eng. 6 (1) (2014) 15–28.
[24] J.A. Zakeri, M. Esmaeili, S. Mosayebi, R. Abbasi, Effects of vibration in desert area caused by moving trains, J. Modern Transp. 20 (1) (2012) 16–23.
[25] China. TMOR. Railway Ballast (TB/T 2140-2008): Railway Industry Standard of the People's Republic of China, 2008.
[26] J. Liu, R. Chen, Z. Liu, G.Z. Liu, P. Wang, X.K. Wei, Comparative analysis of resistance characteristics of composite sleeper and concrete sleeper in ballast bed, Constr. Build. Mater. 300 (2) (2021), 124017.
[27] G.Q. Jing, P. Aela, H. Fu, H. Yin, Numerical and experimental analysis of single tie push tests on different shapes of concrete sleepers in ballasted tracks, Proc. Inst. Mech. Eng. Part F 233 (7) (2019) 666–677.

[28] W. Koc, P. Chrostowski, S. Grulkowski, Tests on lateral resistance in railway tracks during the operation of a tamping machine, Proc. Inst. Mech. Eng. Part F 225 (3) (2011) 325–340.
[29] Z. Zeng, S. Song, W. Wang, B. Xiao, Ballast bed resistance characteristics based on discrete-element modelling, Adv. Mech. Eng. 10 (6) (2018), 168781401878146.
[30] J. Liu, P. Wang, G. Liu, J.L. Xiao, H. Liu, T.C. Gao, Influence of a tamping operation on the vibrational characteristics and resistance-evolution law of a ballast bed, Constr. Build. Mater. 239 (2019), 117879.
[31] S. Laryea, M.S. Baghsorkhi, J.F. Ferelle, G.R. Mcdowell, C. Chen, Comparison of performance of concrete and steel sleepers using experimental and discrete element methods, Transp. Geotech. 1 (4) (2014) 225–240.
[32] X. Ling, H. Xiao, X. Cui, Analysis of mechanical properties of polyurethane-mixed ballast based on energy method, Constr. Build. Mater. 182 (2018) 10–19.
[33] L. Widulinski, R. Kozicki, R. Tejchman, Numerical Simulations of Triaxial Test with Sand Using DEM, Arch. Hydroeng. Environ. Mech. 56 (3–4) (2009) 149–172.
[34] X. Bian, W. Li, Y. Qian, E. Tutumluere, Micromechanical particle interactions in railway ballast through DEM Simulations of direct shear tests, Int. J. Geomech. 19 (5) (2019) 04019031.
[35] S. Lobo-Guerrero, L.E. Vallejo, Discrete element method analysis of rail track ballast degradation during cyclic loading, Granular Matter. 8 (3–4) (2006) 195–204.
[36] W.L. Lim, G.R. Mcdowell, Discrete element modeling of railway ballast, Granular Matter. 7 (1) (2005) 19–29.
[37] Itasca Consulting Group Inc., 2015. PFC 5.0 documentation, User's Guide. Minneapolis.
[38] J. Gong, Z. Nie, Y. Zhu, Z.Y. Liang, X. Wang, Exploring the effects of particle shape and content of fines on the shear behavior of sand-fines mixtures via the DEM, Comput. Geotech. 106 (2018) 161–176.
[39] H. Ahmadi, S.F. Sizkow, Numerical analysis of ground improvement effects on dynamic settlement of uniform sand using DEM, SN Appl. Sci. 2 (2020) 689.
[40] G. Jing, X. Zhang, W. Jia, Lateral resistance of polyurethane-reinforced ballast with the application of new bonding schemes: Laboratory tests and discrete element simulations, Constr. Build. Mater. 221 (10) (2019) 627–636.
[41] H.G. Jiang, X.C. Bian, Y.M. Chen, J.Q. Jiang, Full-scale accelerated testing for simulation of train moving loads in track-subgrade system of high-speed railways, China Civil Eng. J. 48 (9) (2015) 85–95 (in Chinese).
[42] F.C. Xue, J.M. Zhang, Attenuations of acceleration spectra of high-speed railway embankment subjected to moving loads, Rock Soil Mech. 36 (2015) 445–451.
[43] E. Tutumluer, Y. Qian, Y.M.A. Hashash, J. Ghaboussi, D.D. Davis, Discrete element modelling of ballasted track deformation behaviour, Int. J. Rail Transp. 1 (2013) 57–73.
[44] Y.L. Guo, W.L. Jia, V. Markine, G.Q. Jing, Rheology study of ballast-sleeper interaction with particle image velocimetry (PIV) and discrete element modelling (DEM), Constr. Build. Mater. 282 (2) (2021), 122710.
[45] A. Danesh, A.A. Mirghasemi, M. Palassi, Evaluation of particle shape on direct shear mechanical behavior of ballast assembly using discrete element method (DEM), Transp. Geotech. 23 (2020), 100357.